

Half moons are pinch points with dispersion

Han Yan (闫寒),^{1,*} Rico Pohle,^{1,†} and Nic Shannon^{1,‡}

¹*Okinawa Institute of Science and Technology Graduate University, Onna-son, Okinawa 904-0412, Japan*

(Dated: December 14, 2024)

“Pinch–points”, singular features observed in (quasi–)elastic neutron scattering, are a widely–discussed hallmark of spin liquids with an emergent gauge symmetry. Much less attention has been paid to “half–moons”, distinctive crescent patterns at finite energy, which have been observed observed in experiments on a number of pyrochlore magnets, and in a wide range of model calculations. Here we unify these two phenomena within a single framework, paying particular attention to the case of ordered, or field–saturated, states where gauge symmetry is explicitly broken, but pinch points and half moons can still be found in dispersing bands of excitations above a gap. We find the half moons are nothing other than pinch–points inscribed on a dispersing band, and act as witness to the same (proximate) gauge symmetry. Molecular dynamics simulations of the Kagome–lattice antiferromagnet are used to explore how these bands of excitations evolve into the ground state and excitations of a classical spin liquid, once gauge symmetry is restored. We explicitly demonstrate that this theory can reproduce the pinch points and half moons observed in the excitations of $\text{Nd}_2\text{Zr}_2\text{O}_7$.

A central challenge in the study of frustrated magnets is to identify features which can be used to distinguish between different types of magnetic state, in the absence of conventional long–range magnetic order [1, 2]. In this context, any robust feature observed in more than one system is of potential interest as a witness to the underlying physics. A prime example is provided by “pinch points”; singular, bow–tie like motifs in the spin structure factor, characteristic of “Coulombic” phases with an underlying gauge symmetry [3–7]. Pinch points have famously been observed in neutron–scattering experiments on spin ice [8], a wide range of other pyrochlore magnets [9, 10], and in simulations of, e.g., Kagome–lattice antiferromagnets [11, 12].

Another characteristic feature, often observed in parallel with pinch points, are the split rings of scattering found at finite energy in $\text{Tb}_2\text{Ti}_2\text{O}_7$ [13, 14]; in the excitations of the “proximate” spin–liquid $\text{Nd}_2\text{Zr}_2\text{O}_7$ [15, 16], and in numerical simulations of a wide range of frustrated magnets, where they have been described to as “excitation rings” [17], “spherical surfaces” [18], and “half moons” [19, 20]. However, despite being documented a decade ago [17], the connection between pinch points found at low energy, and the half moons observed at higher energy, remains obscure.

In this Communication, we establish a unified theory of pinch points and half moons, considering the simplest model which exhibits both features in its dynamical structure factor; the Heisenberg antiferromagnet (HAF) on a Kagome lattice, with magnetisation saturated by applied magnetic field. Introducing a description in terms of continuum fields, we show that pinch points and half moons arise from the divergence–free and curl–free components of the same, emergent, magnetic field. Regular pinch points arise from the divergence–free condition, and the associated spin excitations form a flat band. In

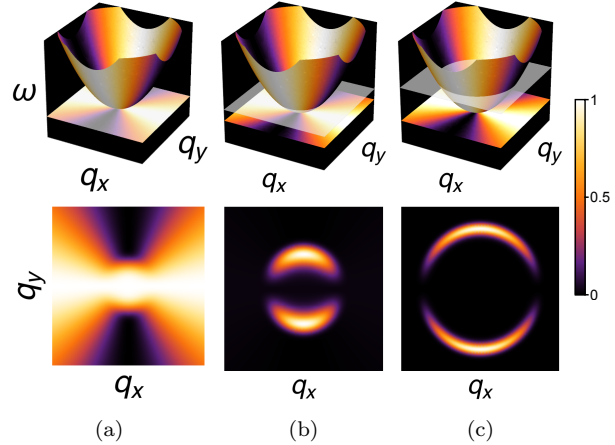


FIG. 1. Illustration of connection between pinch points and half moons, as found in the saturated phase of the Heisenberg antiferromagnet (HAF) on a Kagome lattice, in applied magnetic field. Upper panels: flat and dispersing bands of spin excitations, showing cross–sections at fixed energy (white plane). Lower panels: corresponding prediction for the dynamical structure factor at fixed energy. Pinch–point singularities are encoded in both the flat, and the dispersing band, where they appear as half–moon features. Results have been calculated within a continuum field theory, described below, and convoluted with a Gaussian envelope, to mimic the effect of finite energy resolution.

the case of the curl–free component, excitations form a dispersing band, while the intensity of the associated scattering is modulated in the same way as for a (rotated) pinch point. The combination of these two effects leads to characteristic half–moon features in correlations at fixed energy — a phenomenology summarised in Fig. 1.

We further use molecular dynamics (MD) simulation to explore the fate of pinch–points and half–moons in

the absence of magnetic field. Finally, we discuss the relevance of these results to real materials, using our theory to develop explicit predictions for the pinch points and half moons observed in $\text{Nd}_2\text{Zr}_2\text{O}_7$, in excellent agreement with experiment.

The model — We take as a starting point the HAF on a Kagome lattice

$$\mathcal{H} = J \sum_{\langle i,j \rangle} \mathbf{S}_i \cdot \mathbf{S}_j - H \sum_i S_i^z \quad (1)$$

and consider first the case $H > 6J$, where the ground state has been saturated by magnetic field [21]. Here the one-magnon excitation spectrum can be calculated exactly using linear spin wave (LSW) theory. For $H = 10J$, this leads to the results shown in Fig. 2. There are three inequivalent bands of excitations; a flat band at $\omega = 4J$, and two dispersing bands spanning energies $4J \leq \omega \leq 10J$. The flat band encodes pinch points, clearly seen in the dynamical structure factor $S(\omega, \mathbf{q})$ for $\omega = 4J$ [Fig. 2i]. Meanwhile, dispersing bands exhibit half-moon features, which “grow out” from those zone centers where pinch points are found at low energy [Fig. 2f]. The question is, how are these features connected?

We can answer this question by introducing a continuum field theory description of the magnetic excitations. We consider only the spin components perpendicular to the magnetization, $\nu = x, y$, and group these into two vector and two scalar fields

$$\mathbf{m}_\nu = \sum_{i=1}^3 S_i^\nu \mathbf{u}_i \quad , \quad \xi_\nu = \sum_{i=1}^3 S_i^\nu \quad , \quad (2)$$

where the sum runs over the sites of a primitive unit cell, and the unit vectors

$$\mathbf{u}_1 = (0, 1), \mathbf{u}_2 = (-\sqrt{3}/2, 1/2), \mathbf{u}_3 = (\sqrt{3}/2, 1/2) \quad . \quad (3)$$

It follows that the fields ξ_ν and \mathbf{m}_ν [Eq. (2)] transform with the A_1 and E irreps of the primitive unit cell, respectively [22]. We can further separate the vector fields \mathbf{m}_ν into curl–full and divergence–full components by Helmholtz–Hodge decomposition [23]:

$$\mathbf{m}_\nu = \mathbf{m}_\nu^{\text{curl}} + \mathbf{m}_\nu^{\text{div}} \quad , \quad \mathbf{m}_\nu^{\text{curl}} = \nabla_\perp a_\nu \quad , \quad \mathbf{m}_\nu^{\text{div}} = -\nabla \phi_\nu \quad , \quad (4)$$

where a_ν and ϕ_ν are two scalar potentials and, in two dimensions, the curl and divergence are defined through

$$\nabla_\perp = (-\partial_y, \partial_x) \quad , \quad \nabla = (\partial_x, \partial_y) \quad . \quad (5)$$

This decomposition of the fields has much in common with the “moment fragmentation” explored in the context of pyrochlore magnets [24, 25], and the fact that $\mathbf{m}_\nu^{\text{curl}}$ obeys a zero–divergence condition naturally motivates the introduction of a $U(1)$ gauge field. It is also interesting to note that, within this picture, the field

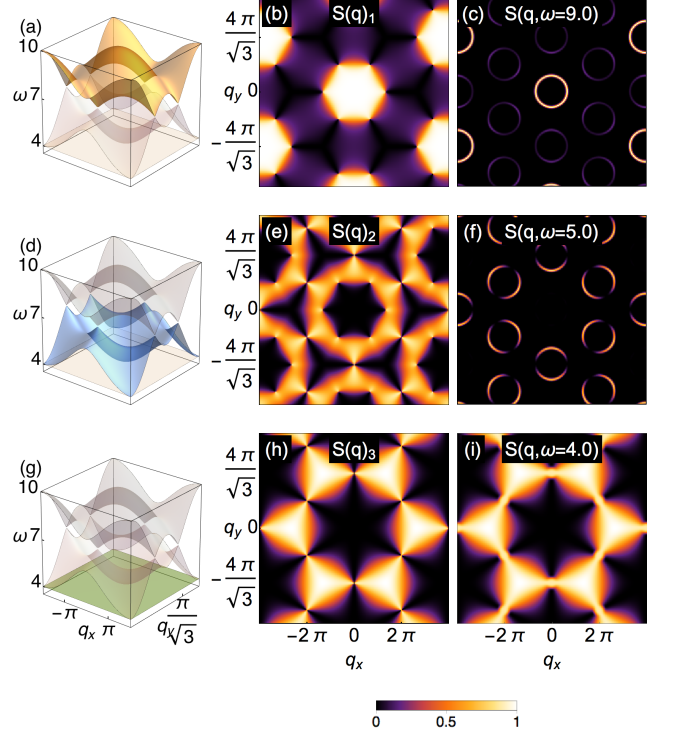


FIG. 2. Spin-wave excitations of the Heisenberg antiferromagnet (HAF) on a Kagome lattice in high magnetic field, showing associated pinch-point and half-moon features. (a) Dispersion of upper band of excitations for $7 \leq \omega \leq 10$. (b) Contribution to equal-time structure factor, $S(\mathbf{q})$, coming from integration over upper band of excitations. (c) Dynamical structure factor $S(\mathbf{q}, \omega)$ evaluated at $\omega = 9.0$, showing rings of scattering. (d)–(f) Corresponding results for middle band of excitations, showing half-moon features at $\omega = 5.0$. (g)–(i) Corresponding results for flat band of excitations, showing pinch-point features at $\omega = 4.0$. All results were obtained within linear spin wave (LSW) theory for Eq. (1), with $J = 1$ and $H = 10$.

$\mathbf{m}_\nu^{\text{div}}$ is associated with the existence of point-like magnetic charges, i.e. magnetic monopoles. However within the high-field saturated state, all excitations are gapped, implying that gauge symmetry is broken.

Origin of pinch points — Following [25], we can now analyse spin-dynamics through the Heisenberg equations of motion (EoM), an approach which is expected to be exact for the one-magnon band at zero temperature. Eq. (4) leads to a remarkable simplification in the EoM, with $\mathbf{m}_\nu^{\text{curl}}$ decoupling from other fields entirely, to give

$$\partial_t a_x = \omega_0 a_y \quad , \quad \partial_t a_y = -\omega_0 a_x \quad , \quad (6)$$

where here and below, we set $\hbar = 1$. This implies the existence of a flat band of excitations with energy

$$\omega^{\text{curl}}(\mathbf{q}) = \omega_0 = H - 6J \quad . \quad (7)$$

The structure of correlations within this band are determined by the condition $\nabla \cdot \mathbf{m}_\nu^{\text{curl}} = 0$. In momentum

space, this implies $\mathbf{q} \cdot \mathbf{m}_\nu^{\text{curl}} = 0$, and the associated dynamical structure factor is given by

$$\langle m_{\nu,\alpha}^{\text{curl}}(\mathbf{q}, \omega) m_{\nu',\beta}^{\text{curl}}(-\mathbf{q}, \omega) \rangle \propto \delta_{\nu\nu'} \delta(\omega - \omega_0) (1 - q_\alpha q_\beta / \mathbf{q}^2), \quad (8)$$

where $\alpha, \beta = x, y$ are the spatial components of the vector fields $\mathbf{m}_\nu^{\text{curl}}$ and $\mathbf{m}_{\nu'}^{\text{curl}}$ defined in Eq. (4). It follows that the intensity of scattering has the familiar structure of a pinch point [5]. A parallel analysis, leading to pinch points on a flat band at finite energy, has been given by Benton [25] in the context of $\text{Nd}_2\text{Zr}_2\text{O}_7$, a case which we return to below.

Origin of half moons — We now turn to the dynamics of the field $\mathbf{m}_\nu^{\text{div}}$. In this case the relevant EoM are given by

$$\partial_t \phi_x = [\omega_0 + D\nabla^2] \phi_y, \quad \partial_t \phi_y = [-\omega_0 - D\nabla^2] \phi_x \quad (9)$$

yielding a band with quadratic dispersion

$$\omega^{\text{div}}(\mathbf{q}) = \omega_0 + D\mathbf{q}^2, \quad D = J/4. \quad (10)$$

The structure of correlations within this band are determined by the condition $\nabla_\perp \cdot \mathbf{m}_\nu^{\text{div}} = 0$. This implies

$$\tilde{\mathbf{q}} \cdot \mathbf{m}_\nu^{\text{div}} = 0, \quad \tilde{\mathbf{q}} = (-q_y, q_x), \quad (11)$$

and the corresponding dynamical structure factor is given by

$$\langle m_{\nu,\alpha}^{\text{div}}(\mathbf{q}, \omega) m_{\nu',\beta}^{\text{div}}(-\mathbf{q}, \omega) \rangle \propto \delta_{\nu\nu'} \delta(\omega - \omega_0 - D\mathbf{q}^2) \times (1 - \tilde{q}_\alpha \tilde{q}_\beta / \mathbf{q}^2). \quad (12)$$

These correlations also have the form of a pinch point, but this is now imprinted on a dispersing band, and orientated perpendicular to the “conventional” pinch point in the flat band [Eq. (8)].

The reason for the appearance of “half moons” in dynamical structure factors now becomes evident. In cuts taken at constant energy, the band of excitations associated with $\mathbf{m}_\nu^{\text{div}}$ appear as rings of scattering satisfying $\omega = \omega^{\text{div}}(\mathbf{q})$, but with intensity which vanishes approaching a characteristic line in reciprocal space [cf. Eq. (12)]. This converts a single ring into two, symmetrical, crescent features, aka “half moons”. In the case of the spin structure factor, $S(\mathbf{q}, \omega)$, the orientation of the half-moons depends on which component of $\mathbf{m}_\nu^{\text{div}}$ is probed in a given Brillouin zone (BZ) [Fig. 2f]. However, within any given BZ, the half-moon feature is orthogonal to the pinch point in the accompanying flat band [Fig. 2i]. This generic structure, of half moons (associated with a field satisfying a zero-curl condition), dispersing out of zone center where they meet a flat band (associated with a field satisfying a zero-divergence condition), is illustrated in Fig. 1a–1c.

The results of this field theory [Fig. 1] perfectly reproduce LSW calculations [Fig. 2], in the relevant long-wavelength limit. Comparing the separate contribution of each spin-wave band to the equal-time structure factor

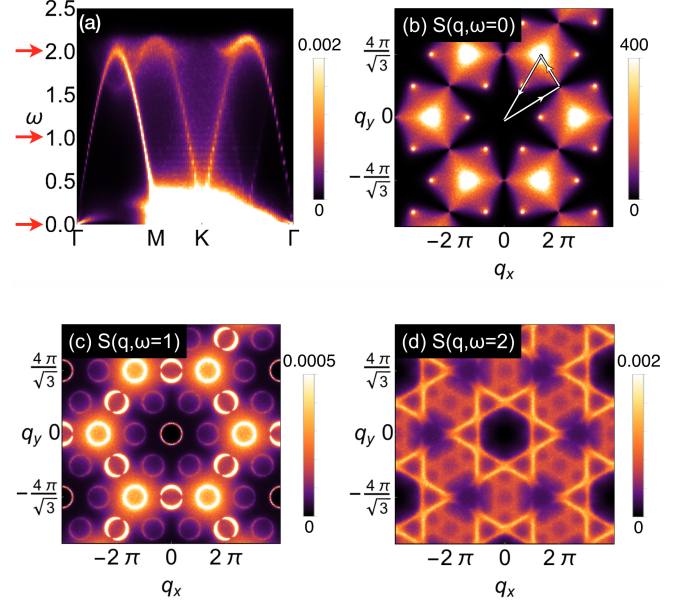


FIG. 3. Dynamical structure factor found in molecular dynamics (MD) simulations of the Kagome antiferromagnet in absence of magnetic field, showing persistence of half-moon features. (a) Results for the dynamical structure factor $S(\omega, \mathbf{q})$ at $T = 0.001 J$, on an irreducible wedge of the BZ. Energies used for cross sections at fixed ω are marked with red arrows. (b)–(d) Dynamical structure of HAF at $\omega = 0, 1, 2$, showing evolution of half-moons out of a flat band encoding pinch points at zero energy. Details of simulations are given in the Supplementary Materials.

$S(\mathbf{q}) = \int d\omega S(\mathbf{q}, \omega)$, we again see that the pinch points of the dispersing band [Fig. 2e], are perpendicular to those of the flat band [Fig. 2h], with the total spectral weight at each \mathbf{q} satisfying a sum rule across the three bands.

“Half moons” in the absence of magnetic field — So far, we have limited our discussion to gapped excitations about a field-saturated state. None the less, molecular-dynamics (MD) simulations have also revealed half-moon structures in the excitations of a (classical) spin-liquid on Kagome lattice in the absence of magnetic field [12, 17], and it is interesting to ask how pinch points and half moons evolve, once the gap to spin excitations closes.

In Fig. 3 we show MD results in the absence of magnetic field ($H = 0$). We find a spin-liquid ground state, formed when the gap to the flat band closes [21] at the critical field $H_c = 6J$. Half-moon features survive at finite energy [Fig. 3c], with intensity perpendicular to the pinch points in the static structure factor [Fig. 3b]. The bands carrying half moons evolve smoothly out of the excitations of the field-saturated state, and the structure of the half moons remains well-described by Eq. (12). These results are consistent with the restoration of an emergent $U(1)$ gauge symmetry at the field $H = H_c$. And in this context, it is interesting to recall that the curl-free excitations, which give rise to half moons, re-

flect the field coming from a magnetic monopole [Eq. (4)].

Experimental realizations — The most straightforward experimental application of these ideas is to $\text{Nd}_2\text{Zr}_2\text{O}_7$, a pyrochlore magnet in which a Nd^{3+} moment is “fragmented”, so that a magnetically ordered ground state is accompanied by a “dynamical spin liquid”, with flat band encoding spin-ice like pinch points above a finite energy gap [15]. At higher energies inelastic neutron scattering experiments perfectly capture the pattern of half moons on a quadratically-dispersing band, evolving out of the pinch points of the flat band (cf. Fig. S3 of [15]). The microscopic structure of EoM for spin excitations in $\text{Nd}_2\text{Zr}_2\text{O}_7$, as well as parameters for a microscopic model, have already been discussed by Benton [25]. What remains is to show that a field-theory of the type developed in this Communication can reproduce the scattering seen in experiment.

In Fig. 4, we present explicit field-theory predictions for $\text{Nd}_2\text{Zr}_2\text{O}_7$, following the pattern developed above (see Supplemental Materials). The field theory has been parameterised from the microscopic model of [25], with overall intensity and experimental resolution determined from a fit to the elastic line in Fig. 4(a) of [15], leaving no adjustable parameters. The agreement, for the long-wavelength features described by our field theory, is excellent, confirming that half-moon features originate in a dispersing band of excitations satisfying a zero-curl condition. We note that behaviour consistent with half-moon features dispersing out of a flat band has also been observed for $\text{Nd}_2\text{Zr}_2\text{O}_7$ in a magnetic field parallel to the [111] axis, where it is expected to realise a dynamic quantum Kagome ice [16].

$\text{Tb}_2\text{Ti}_2\text{O}_7$, another Pyrochlore oxide, comes with more complication [13, 14, 26, 27]. In [13], a dispersive band with half moons is observed at very low energy scale from 0.0 to 0.3 meV, attaching to the pinch-point band at zero energy. Remarking on these, the authors of [13] conjectured that the half moons “could be an intrinsic feature of Coulomb phases”, which “will have to be confirmed in further theoretical studies”. The results in this Communication suggest that half moons are indeed intimately related to the gauge structure of Coulomb phases. As there is no established microscopic model for $\text{Tb}_2\text{Ti}_2\text{O}_7$, it is not possible to carry out the same kind of quantitative analysis as for $\text{Nd}_2\text{Zr}_2\text{O}_7$. Nonetheless, it might be interesting to apply a phenomenology of the form of Eq (12) to inelastic neutron scattering data.

Lastly, we turn to $\text{Ca}_{10}\text{Cr}_7\text{O}_{28}$, a recently-discovered material realising a spin-1/2 Heisenberg model on a bilayer breathing-Kagome (BBK) lattice, which supports a quantum spin liquid ground state [28]. Here once again, inelastic neutron scattering carried out in magnetic field reveals both flat and dispersing bands at finite energy, with evidence for pinch-point structure within the flat band [29]. Both numerical simulations and spin-wave calculations [30], parameterised from

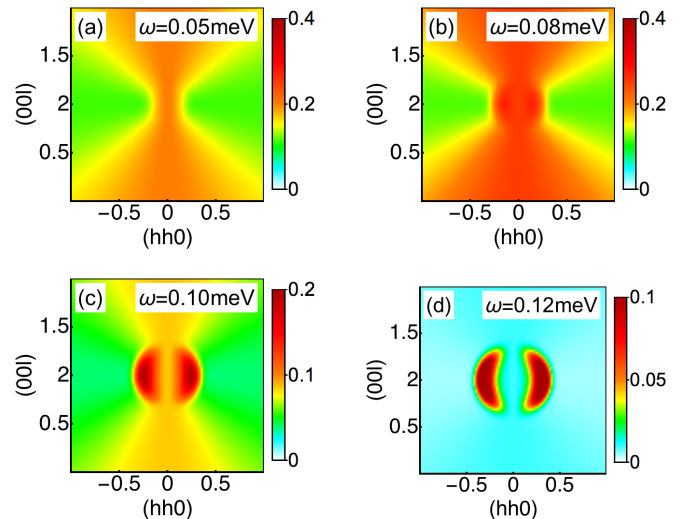


FIG. 4. Predictions for the dynamical structure factors of the proximate spin liquid $\text{Nd}_2\text{Zr}_2\text{O}_7$, calculated from a continuum field theory with $U(1)$ gauge structure. The analysis has been parameterised from experiment [15, 25], leaving no adjustable parameters. Approaching the zone center, the agreement with inelastic neutron scattering is excellent (cf. Fig. S3 of [15]). Details of the analysis are given in the Supplementary Materials.

experiment [29], reveal distinct half-moon features dispersing out of the pinch points of the flat band, consistent with the framework in this Communication. We therefore anticipate that more detailed measurements of the dispersing bands of $\text{Ca}_{10}\text{Cr}_7\text{O}_{28}$ in high field will reveal half-moon features.

Summary and Conclusions — In this Communication we have explored the connection between pinch points — singular features in neutron scattering associated with both Coulombic spin liquids and flat bands of excitations in frustrated magnets; and “half moons” — characteristic crescent features in inelastic scattering which are frequently found accompanying pinch points. We find that half moons are nothing but a second set of pinch points with dispersion [Fig. 1]. Considering the specific example of the Heisenberg antiferromagnet on a Kagome lattice, in applied magnetic field [Fig. 2], we show that the connection between pinch points and half moons can be made explicit through a Helmholtz decomposition of the associated spin configurations, implying that they originate in the same, proximate, $U(1)$ gauge symmetry. While our field-theoretic analysis is limited to excitations of a field-saturated state, we expect the same considerations to apply to classical spin liquids, and find evidence in MD simulation to reinforce this claim [Fig. 3]. Finally, we have discussed the application of these ideas to the frustrated magnets $\text{Tb}_2\text{Ti}_2\text{O}_7$ and $\text{Ca}_{10}\text{Cr}_7\text{O}_{28}$, and demonstrate that they quantitatively reproduce the

half-moon features found in $\text{Nd}_2\text{Zr}_2\text{O}_7$ [Fig. 4].

We conclude with a few comments about interesting open problems. Half moons have also been observed in models without explicit dynamics [18–20]. Here, the same basic mechanism, of pinch points “bent up” in energy, presumably applies. However alternative methods would be needed to elaborate how this happens. Another important open problem is the fate of half moons in a fully-entangled quantum spin liquid (QSL). In this context, it is interesting to ask how the pinch points and half moons of proximate spin liquid $\text{Nd}_2\text{Zr}_2\text{O}_7$ would evolve, if it were possible to close the gap to the flat band of excitations carrying pinch points [15, 25]. In this case we anticipate that the flat band will evolve into the photons of a quantum spin ice [25], while the dispersing band carrying the half moons must connect with its topological, “magnetic monopole” excitations [31]. Explicit calculations for QSL’s, however, remain to be carried out. Finally, while completing this work, we learned of a parallel study by Mizoguchi *et al.*, which reports complementary results for a different model [32].

Acknowledgements — This work was supported by the Theory of Quantum Matter Unit, Okinawa Institute of Science and Technology Graduate University (OIST). The authors would like to thank Owen Benton, Bella Lake, Mathieu Taillefumier, and Alexandra Turrini for helpful discussions. Numerical calculations are carried out using HPC Facilities provided by OIST. HY thanks the Yukawa Institute for Theoretical Physics at Kyoto University, where part of this work was done during the workshop “Novel Quantum States in Condensed Matter 2017” (NQS2017, YITP-T-17-01).

* han.yan@oist.jp
 † rico.pohle@oist.jp
 ‡ nic.shannon@oist.jp

[1] L. Balents, *Nature* **464**, 199 (2010).
 [2] L. Savary and L. Balents, *Reports on Progress in Physics* **80**, 016502 (2017).
 [3] R. Moessner and J. T. Chalker, *Phys. Rev. B* **58**, 12049 (1998).
 [4] D. A. Huse, W. Krauth, R. Moessner, and S. L. Sondhi, *Phys. Rev. Lett.* **91**, 167004 (2003).
 [5] C. L. Henley, *Annual Review of Condensed Matter Physics* **1**, 179 (2010).
 [6] O. Benton, L. Jaubert, H. Yan, and N. Shannon, *Nature Communications* **7**, 11572 (2016).
 [7] A. Prem, S. Vijay, Y.-Z. Chou, M. Pretko, and R. M. Nandkishore, ArXiv:1806.04148.
 [8] T. Fennell, P. P. Deen, A. R. Wildes, K. Schmalzl, D. Prabhakaran, A. T. Boothroyd, R. J. Aldus, D. F. Morrow, and S. T. Bramwell, *Science* **326**, 415 (2009).
 [9] T. Fennell, M. Kenzelmann, B. Roessli, M. K. Haas, and R. J. Cava, *Phys. Rev. Lett.* **109**, 017201 (2012).
 [10] R. Sibille, N. Gauthier, H. Yan, M. C. Hatnean, J. Olivier, B. Winn, U. Filges, G. Balakrishnan, M. Ken-

zelmann, N. Shannon, and T. Fennell, *Nature Physics* doi:10.1038/s41567-018-0116-x.

[11] M. E. Zhitomirsky, *Phys. Rev. B* **78**, 094423 (2008).
 [12] M. Taillefumier, J. Robert, C. L. Henley, R. Moessner, and B. Canals, *Phys. Rev. B* **90**, 064419 (2014).
 [13] S. Guitteny, J. Robert, P. Bonville, J. Ollivier, C. Decorse, P. Steffens, M. Boehm, H. Mutka, I. Mirebeau, and S. Petit, *Phys. Rev. Lett.* **111**, 2 (2013).
 [14] T. Fennell, M. Kenzelmann, B. Roessli, H. Mutka, J. Olivier, M. Rumin, U. Stuhr, O. Zaharko, L. Bovo, A. Cervellino, M. K. Haas, and R. J. Cava, *Phys. Rev. Lett.* **112**, 017203 (2014).
 [15] S. Petit, E. Lhotel, B. Canals, M. Ciomaga Hatnean, J. Ollivier, H. Mutka, E. Ressouche, A. R. Wildes, M. R. Lees, and G. Balakrishnan, *Nature Physics* **12**, 746 (2016).
 [16] E. Lhotel, S. Petit, M. C. Hatnean, J. Ollivier, H. Mutka, E. Ressouche, M. R. Lees, and G. Balakrishnan, (2017), arXiv:1712.02418.
 [17] J. Robert, B. Canals, V. Simonet, and R. Ballou, *Phys. Rev. Lett.* **101**, 117207 (2008).
 [18] J. G. Rau and M. J. P. Gingras, *Nature Communications* **7**, 12234 (2016).
 [19] M. Udagawa, L. D. Jaubert, C. Castelnovo, and R. Moessner, *Phys. Rev. B* **94**, 104416 (2016).
 [20] T. Mizoguchi, L. D. C. Jaubert, and M. Udagawa, *Phys. Rev. Lett.* **119**, 077207 (2017).
 [21] M. E. Zhitomirsky, *Phys. Rev. Lett.* **88**, 057204 (2002).
 [22] K. Essafi, O. Benton, and L. D. C. Jaubert, *Phys. Rev. B* **96**, 205126 (2017).
 [23] G. B. Arfken and H. J. Weber, *Mathematical Methods for Physicists* (Academic Press: San Diego, 1995).
 [24] M. E. Brooks-Bartlett, S. T. Banks, L. D. Jaubert, A. Harman-Clarke, and P. C. Holdsworth, *Phys. Rev. X* **4**, 011007 (2014).
 [25] O. Benton, *Phys. Rev. B* **94**, 104430 (2016).
 [26] M. Rumin, E. Pomjakushina, K. Iida, K. Kamazawa, D. T. Adroja, U. Stuhr, and T. Fennell, *Phys. Rev. B* **94**, 214308 (2016).
 [27] M. Rumin, M. N. Valdez, B. Wehinger, A. Bosak, D. T. Adroja, U. Stuhr, K. Iida, K. Kamazawa, E. Pomjakushina, D. Prabhakaran, M. K. Haas, L. Bovo, D. Sheptyakov, A. Cervellino, R. J. Cava, M. Kenzelmann, N. A. Spaldin, and T. Fennell, *Phys. Rev. B* **93**, 214308 (2016).
 [28] C. Balz, B. Lake, J. Reuther, H. Luetkens, R. Schonemann, T. Herrmannsdorfer, Y. Singh, A. T. M. Nazmul Islam, E. M. Wheeler, J. A. Rodriguez-Rivera, T. Guidi, G. G. Simeoni, C. Baines, and H. Ryll, *Nature Physics* **12**, 942 (2016).
 [29] C. Balz, B. Lake, A. T. M. Nazmul Islam, Y. Singh, J. A. Rodriguez-Rivera, T. Guidi, E. M. Wheeler, G. G. Simeoni, and H. Ryll, *Phys. Rev. B* **95**, 174414 (2017).
 [30] R. Pohle, H. Yan, and N. Shannon, (2017), arXiv:1711.03778.
 [31] C.-J. Huang, Y. Deng, Y. Wan, and Z. Y. Meng, *Phys. Rev. Lett.* **120**, 167202 (2018).
 [32] T. Mizoguchi, L. D. C. Jaubert, and M. Udagawa, Private communication.

Supplementary Materials for Half moons are pinch points with dispersion

Han Yan (闫寒),^{1,*} Rico Pohle,^{1,†} and Nic Shannon^{1,‡}

¹*Okinawa Institute of Science and Technology Graduate University, Onna-son, Okinawa 904-0412, Japan*

(Dated: June 22, 2018)

I. KAGOME LATTICE MODEL AND ASSOCIATED EQUATIONS OF MOTION

We consider a Heisenberg model on a Kagome lattice

$$\mathcal{H} = J \sum_{\langle ij \rangle} \mathbf{S}_i \cdot \mathbf{S}_j - H \sum_i S_i^z, \quad (1)$$

where $H > 0$ is the applied magnetic field, $J > 0$ is an antiferromagnetic exchange interaction, and the sum $\langle ij \rangle$ runs over the nearest-neighbor bonds of the lattice, shown in Fig. 1.

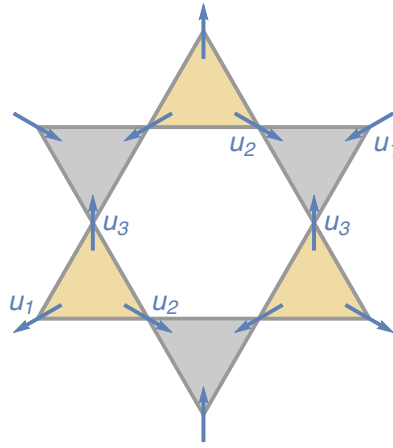


FIG. 1. Kagome lattice associated with the Heisenberg model \mathcal{H} [Eq. (1)], and associated vectors \mathbf{u}_i [Eq. (5)], used in decomposition of fields [Eq. (4)].

The Heisenberg equations of motion (EoMs) for a spin $\mathbf{S}_i = (S_i^x, S_i^y, S_i^z)$ on this lattice are given by

$$\frac{d\mathbf{S}_i}{dt} = \frac{i}{\hbar} [\mathcal{H}, \mathbf{S}_i], \quad (2)$$

where, in what follows, we set $\hbar = 1$.

The primitive unit cell for the Kagome lattice contains three spins, denoted $\mathbf{S}_i, i = 1, 2, 3$. For $H \gg J$, the ground state is saturated as $\langle S_i^z \rangle = 1$, $\langle S_i^{x,y} \rangle = 0$. At linear order, there are six degrees of freedom in each unit cell, namely S_i^x, S_i^y for $i = 1, 2, 3$. Their EoMs are

$$\begin{aligned} \partial_t S_i^x &= -J \sum_j (S_j^y - S_i^y) + S_i^y H, \\ \partial_t S_i^y &= -J \sum_j (S_j^x - S_i^x) - S_i^x H. \end{aligned} \quad (3)$$

* han.yan@oist.jp

† rico.pohle@oist.jp

‡ nic.shannon@oist.jp

II. EQUATIONS OF MOTION FOR CONTINUOUS FIELDS

The six degrees of freedom S_i^x, S_i^y for $i = 1, 2, 3$ in each unit cell can be reorganized as irreducible representations of the lattice symmetry:

$$\begin{aligned}\mathbf{m}_x &= \sum_{i=1}^3 S_i^x \mathbf{u}_i, \quad \xi_x = \sum_{i=1}^3 S_i^x, \\ \mathbf{m}_y &= \sum_{i=1}^3 S_i^y \mathbf{u}_i, \quad \xi_y = \sum_{i=1}^3 S_i^y,\end{aligned}\quad (4)$$

where

$$\mathbf{u}_1 = (-\sqrt{3}/2, -1/2), \quad \mathbf{u}_2 = (\sqrt{3}/2, -1/2), \quad \mathbf{u}_3 = (0, 1), \quad (5)$$

are local unit vectors to help us build the irreducible representations [cf Fig 1]. Note here x, y in the subscript denote different fields, not their spatial components. The explicit expressions for \mathbf{m}_x and \mathbf{m}_y are

$$\begin{aligned}\mathbf{m}_x &= (\sqrt{3}/2(-S_1^x + S_2^x), -S_1^x/2 - S_2^x/2 + S_3^x), \\ \mathbf{m}_y &= (\sqrt{3}/2(-S_1^y + S_2^y), -S_1^y/2 - S_2^y/2 + S_3^y).\end{aligned}\quad (6)$$

We can rewrite the discrete, microscopic EoMs [Eq. 3] in the continuous limit in terms of \mathbf{m}_ν and ξ_ν :

$$\begin{aligned}\partial_t \mathbf{m}_x &= \frac{J}{4} \nabla(\nabla \cdot \mathbf{m}_y) + \tilde{H} \mathbf{m}_y, \\ \partial_t \mathbf{m}_y &= -\frac{J}{4} \nabla(\nabla \cdot \mathbf{m}_x) - \tilde{H} \mathbf{m}_x, \\ \partial_t \xi_x &= -\frac{J}{4} \nabla^2 \xi_y + H \xi_y, \\ \partial_t \xi_y &= \frac{J}{4} \nabla^2 \xi_x - H \xi_x,\end{aligned}\quad (7)$$

where $\tilde{H} = H - 6J$. We note that the definitions of divergence and curl in two dimension, shown in Table I, are slightly different from those in three dimensions.

TABLE I. Summary of definitions of divergence/gradient and curl/scalar curl in 2D.

	Notation	Definition	Acting on vector field \mathbf{v}	Acting on scalar field ϕ
Divergence/gradient	∇	(∂_x, ∂_y)	$\partial_x v_x + \partial_y v_y$	$(\partial_x \phi, \partial_y \phi)$
Curl/scalar curl	∇_\perp	$(-\partial_y, \partial_x)$	$-\partial_y v_x + \partial_x v_y$	$(-\partial_y \phi, \partial_x \phi)$

Except for the constant energy shift terms with coefficient \tilde{H} or H , all terms on the right hand side of the EoM are of the form ∇ acting on a scalar or vector field. This property of the EoMs suggests that we can decompose \mathbf{m}_ν into $\mathbf{m}_\nu^{\text{curl}}$ and $\mathbf{m}_\nu^{\text{div}}$, by standard Helmholtz-Hodge decomposition [1],

$$\mathbf{m}_\nu = \mathbf{m}_\nu^{\text{curl}} + \mathbf{m}_\nu^{\text{div}}, \quad (8)$$

where

$$\mathbf{m}_\nu^{\text{curl}} = \nabla_\perp a_\nu, \quad \mathbf{m}_\nu^{\text{div}} = \nabla \phi_\nu, \quad (9)$$

and a_ν, ϕ_ν are scalar potentials. We note that, in making the decomposition Eq. (8), we have assumed vanishing harmonic components of the field \mathbf{m}_ν . Written in this form, the vector field \mathbf{m}_ν has two components, which are characterised by the two fields a_ν and ϕ_ν . And by analogy with magnetostatics, a_ν plays the role of a gauge field, while ϕ_ν corresponds to the potential coming from a magnetic charge.

Exploiting the fact that

$$\nabla_\perp \cdot \mathbf{m}_\nu^{\text{div}} = 0, \quad \nabla \cdot \mathbf{m}_\nu^{\text{curl}} = 0, \quad (10)$$

we can get simplified EoMs, in which the 6 fields $\mathbf{m}_\nu^{\text{curl}}$, $\mathbf{m}_\nu^{\text{div}}$ and ξ_ν all decouple from one other to yield

$$\partial_t \mathbf{m}_x^{\text{curl}} = +\tilde{H} \mathbf{m}_y^{\text{curl}}, \quad \partial_t \mathbf{m}_y^{\text{curl}} = -\tilde{H} \mathbf{m}_x^{\text{curl}}, \quad (11)$$

$$\partial_t \mathbf{m}_x^{\text{div}} = \frac{J}{4} \nabla(\nabla \cdot \mathbf{m}_y^{\text{div}}) + \tilde{H} \mathbf{m}_y^{\text{div}}, \quad \partial_t \mathbf{m}_y^{\text{div}} = -\frac{J}{4} \nabla(\nabla \cdot \mathbf{m}_x^{\text{div}}) - \tilde{H} \mathbf{m}_x^{\text{div}}, \quad (12)$$

$$\partial_t \xi_x = -\frac{J}{4} \nabla^2 \xi_y + H \xi_y, \quad \partial_t \xi_y = \frac{J}{4} \nabla^2 \xi_x - H \xi_x. \quad (13)$$

Conventional pinch points are encoded in the field $\mathbf{m}_\nu^{\text{curl}}$. For the purpose of understanding these we can use Eq. (9) to rewrite Eq. (11) in terms of a_ν . This leads to the result

$$\partial_t a_x = \omega_0 a_y, \quad \partial_t a_y = -\omega_0 a_x, \quad (14)$$

quoted in the Main Text. Meanwhile, “half moons” are encoded in the field $\mathbf{m}_\nu^{\text{div}}$. And, for the purpose of understanding these, we can use Eq. (9) to rewrite Eq. (12) in terms of a_ν and ϕ_ν . This leads to the result

$$\partial_t \phi_x = [\omega_0 + D \nabla^2] \phi_y, \quad \partial_t \phi_y = [-\omega_0 - D \nabla^2] \phi_x, \quad (15)$$

quoted in the Main Text.

III. ANALYSIS OF EQUATIONS OF MOTION

A. Dispersion relations

Firstly we examine the dispersion relations which follow from these EoM. In the field–theory approach, the dispersion relations can be obtained by Fourier transforming EoMs [cf Eq. (11), Eq. (12)] into energy–momentum space (\mathbf{q}, ω) , and solving for the eigenvalues ω as a function of \mathbf{q} . This yields

$$\omega_{\text{top}}(\mathbf{q}) = H - \frac{J}{4} \mathbf{q}^2, \quad (16)$$

$$\omega_{\text{mid}}(\mathbf{q}) = \omega_0 + \frac{J}{4} \mathbf{q}^2, \quad (17)$$

$$\omega_{\text{bot}}(\mathbf{q}) = \omega_0, \quad (18)$$

where

$$\omega_0 = \tilde{H} = H - 6J. \quad (19)$$

As discussed in Section IV, equivalent results for the dispersion at long wavelength can also be derived within a standard linear spin–wave calculation.

B. Singular structures in scattering

We now use the field theory to examine the contribution to the equal–time structure factor coming from each band of spin excitations. We consider first the structure factor associated with

$$S_{x,x}^{\text{curl}}(\mathbf{q}) \equiv \langle m_{x,x}^{\text{curl}}(\mathbf{q}) m_{x,x}^{\text{curl}}(-\mathbf{q}) \rangle. \quad (20)$$

The field theory approach developed above leads to the prediction

$$\langle m_{\nu,\alpha}^{\text{curl}}(\mathbf{q}, \omega) m_{\nu',\beta}^{\text{curl}}(-\mathbf{q}, \omega) \rangle \propto \delta_{\nu\nu'} \delta(\omega - \omega_0) (1 - q_\alpha q_\beta / \mathbf{q}^2), \quad (21)$$

where $\omega_0 = H - 6J$, $\alpha, \beta = x, y$ are the spatial components of vector field $\mathbf{m}_\nu^{\text{curl}}$ and $\mathbf{m}_{\nu'}^{\text{curl}}$. Fixing $\alpha = \beta = x = \nu = \nu' = x$, and integrating over ω , we find

$$S_{x,x}^{\text{curl}}(\mathbf{q}) = \langle m_{x,x}^{\text{curl}}(\mathbf{q}) m_{x,x}^{\text{curl}}(-\mathbf{q}) \rangle \propto 1 - \frac{q_x^2}{\mathbf{q}^2}, \quad (22)$$

i.e. a pinch point. As discussed in Section IV, equivalent results can also be derived within a standard linear spin–wave (LSW) calculation.

We now consider the energy-integrated (equal-time) structure factor characterising the dispersing band associated with half moons, i.e.

$$S_{x,x}^{\text{div}}(\mathbf{q}) \equiv \langle m_{x,x}^{\text{div}}(\mathbf{q}) m_{x,x}^{\text{div}}(-\mathbf{q}) \rangle . \quad (23)$$

An analysis similar to that leading to Eq.(22), yields the result quote for the associated dynamical structure factor in Eq. (12) of the main text, i.e.,

$$\langle m_{\nu,\alpha}^{\text{div}}(\mathbf{q}, \omega) m_{\nu',\beta}^{\text{div}}(-\mathbf{q}, \omega) \rangle \propto \delta_{\nu\nu'} \delta(\omega - \omega_0 - D\mathbf{q}^2) \times (1 - \tilde{q}_\alpha \tilde{q}_\beta / \mathbf{q}^2) ,$$

where $D = J/4$. It follows that the field-theory prediction for the energy-integrated structure factor $S_{x,x}^{\text{div}}(\mathbf{q})$ also has the structure of a pinch point

$$S_{x,x}^{\text{div}}(\mathbf{q}) = \langle m_{x,x}^{\text{div}}(\mathbf{q}) m_{x,x}^{\text{div}}(-\mathbf{q}) \rangle \propto 1 - \frac{q_y^2}{\mathbf{q}^2} , \quad (24)$$

but one rotated so as to be perpendicular to the pinch point in Eq. (22). As discussed in Section IV, equivalent results can also be derived within a standard linear spin-wave (LSW) calculation.

IV. COMPARISON BETWEEN FIELD THEORY AND LINEAR SPIN WAVE THEORY

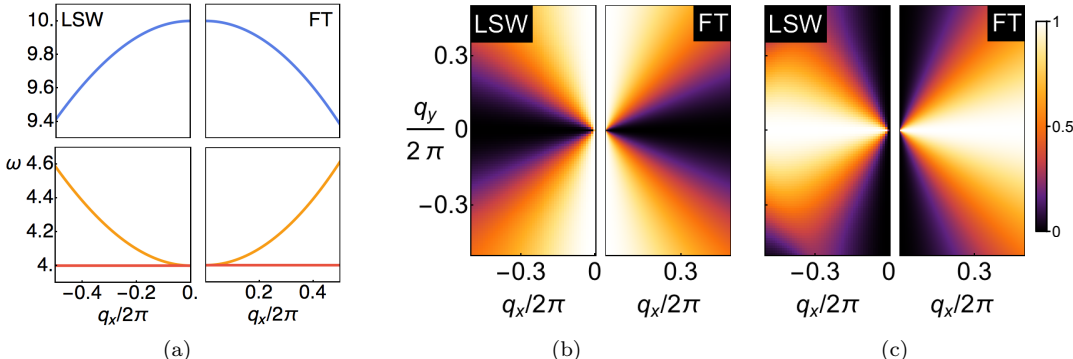


FIG. 2. Comparison of dynamical correlation functions calculated from linear spin wave (LSW) theory and field theory (FT). Results from LSW and FT fit well for a fairly large region near the Γ -point. The calculation is done for parameter $J = 1.0$ and $H = 10.0$. (a) Dispersion of spin excitations along $(q_x, 0)$ near the Γ -point, calculated by LSW (left panel) and field theory (right panel). (b) Equal-time structure factor $S_{x,x}^{\text{curl}}(\mathbf{q})$ [Eq. (20)] calculated within LSW (left panel) and field theory (right panel), showing pinch points associated with the flat band of excitations. (c) Equal-time structure factor $S_{x,x}^{\text{div}}(\mathbf{q})$ [Eq. (23)] calculated within LSW (left panel) and field theory (right panel), showing pinch points associated with the flat band of excitations.

To validate this approach, it is helpful to compare the predictions of the field theory, quoted above, with equivalent results calculated within standard linear spin-wave theory (LSW). We first consider the dispersion relations for the three bands in the vicinity of the Γ -point. The results are summarized in Fig 2a; good agreement is achieved for a wide range of \mathbf{q} centered on the Γ -point.

We can also compare predictions for dynamical structure factors. As a representative case, we can evaluate e.g.

$$\langle m_{x,x}(\omega, \mathbf{q}) m_{x,x}(\omega, -\mathbf{q}) \rangle = \langle \frac{\sqrt{3}}{2} (S_2^x - S_3^x)(\mathbf{q}) \frac{\sqrt{3}}{2} (S_2^x - S_3^x)(-\mathbf{q}) \rangle , \quad (25)$$

using the LSW eigenvectors for the band $\mathbf{m}_\nu^{\text{div}}$ (the dispersing band in the middle of Fig 2(a)). The associated predictions for the equal-time structure factors $S_{x,x}^{\text{curl}}(\mathbf{q})$ and $S_{x,x}^{\text{div}}(\mathbf{q})$, calculated within the two approaches, are shown in Fig 2(b) and Fig 2(c). Once again, the agreement is excellent for a large range of \mathbf{q} centered on the Γ -point.

V. CONNECTION WITH $U(1)$ GAUGE SYMMETRY

A. Gauge Theory from Spin Ice and Square Ice

The physics discussed in this paper is closely related to the breaking of $U(1)$ gauge symmetry. Let us begin by reviewing what is known about spin liquids, using the examples of three-dimensional pyrochlore spin ice and two-dimensional square ice. The issue of confinement is definitely non-trivial, but will not be discussed here.

Microscopically, the ground states are the spin configurations satisfying the two-in-two-out ice rule, written as

$$\nabla \cdot \mathbf{m} = 0 \quad (26)$$

as a consequence of frustration. The divergence free property motivates us to treat \mathbf{m} as a magnetic field, and make the analogy between these classical spin systems and magnetostatics. The ground state spin configurations can be written as

$$\mathbf{m} = \nabla \times \mathbf{A} \quad \text{for spin ice,} \quad (27)$$

$$\mathbf{m} = \nabla_{\perp} a \quad \text{for square ice.} \quad (28)$$

In the case of spin ice, there is an apparent gauge freedom

$$\mathbf{A} \rightarrow \mathbf{A} + \nabla \lambda. \quad (29)$$

In the case of square ice, the gauge freedom is still absent. It only appears when quantum dynamics or electric field is introduced to recover the full electromagnetism, due to the subtlety of 2 + 1 dimensional electromagnetism. However it does not affect most of our discussions.

What matters is that for any two configurations of gauge field \mathbf{A}, \mathbf{A}' or a, a' that are *physically* different,

$$\mathbf{m} = \nabla \times \mathbf{A} \neq \mathbf{m}' = \nabla \times \mathbf{A}' \quad \text{for spin ice,} \quad (30)$$

$$\mathbf{m} = \nabla_{\perp} a \neq \mathbf{m}' = \nabla_{\perp} a' \quad \text{for square ice,} \quad (31)$$

they are still degenerate lowest energy states since the corresponding magnetic field \mathbf{m}, \mathbf{m}' satisfy Eq. (26). In terms of the effective theory, that means the gauge fields cannot have terms that differentiate them in energy, like

$$\mathcal{H}_{\text{mass-spin ice}} = m^2 \mathbf{A}^2, \quad \mathcal{H}_{\text{mass-square ice}} = m^2 a^2, \quad (32)$$

or

$$\mathcal{H}_{\text{prop-spin ice}} = (\nabla \cdot \mathbf{A})^2, \quad \mathcal{H}_{\text{prop-square ice}} = (\nabla a)^2, \quad (33)$$

which are exactly the gauge-symmetry breaking terms. This is expected since we know these spin liquids are described by unbroken $U(1)$ gauge theories.

Phenomenologically, the above physics gives rise to a gapless flat band with pinch-point singularities in the dynamical spin-spin correlation function. The presence of this gap is a result of gauge-symmetry breaking terms of Eq. (32) being absent, and the flatness is a result of terms of Eq. (33) being absent. The pinch points are results of the divergence-free condition of Eq. (26), or more fundamentally of Eq. (27).

Finally, when the proper quantum fluctuation is introduced, the system is allowed to tunnel between different classical ground state configurations. Essentially it introduces a dynamical term for the gauge fields,

$$\mathcal{H}_{\text{dy-spin ice}} = (\dot{\mathbf{A}})^2, \quad \mathcal{H}_{\text{dy-square ice}} = (\dot{a})^2, \quad (34)$$

which plays the role of electric fields. Such quantum tunneling terms will upgrade the classical spin liquid into a quantum spin liquid, and recovers the full electromagnetism.

B. Gauge Symmetry Breaking in Saturated Kagome Model

After establishing the links among the microscopic model, its effective theory, and the phenomena in the dynamical spin-spin correlation function, we are ready to examine what is changed in our model in saturated state.

To begin with, we have an ordered ground state, and no gapless bands. Instead, there is a *gapped* flat band with pinch-point singularities, which corresponds to the excitations satisfying the divergence-free condition of Eq. (26).

This means these excitations can be written as the curl of some gauge field as in Eq. (27). However, the excitations being gapped at

$$\omega = E_0 \quad (35)$$

means one bosonic excitation of gauge field a costs a constant energy. As discussed in the previous sub-section, to capture the physics we have to introduce a term that gives a mass to the gauge field which breaks the gauge symmetry. That is, Eq.(32) has to be included in the effective Hamiltonian. Furthermore, the flatness means that terms in Eq.(33) should still be absent. Therefore, in this model the gauge symmetry is broken explicitly by a term

$$\mathcal{H}_{\text{gauge breaking}} = m^2 a^2, \quad (36)$$

where $m = E_0$. That gap of the flat band indicates the existence of a gauge-symmetry-breaking mass term of the gauge field.

VI. APPLICATION TO $\text{Na}_2\text{Zr}_2\text{O}_7$

The field theory developed in the Main Text is sufficient to reproduce inelastic neutron scattering results of $\text{Nd}_2\text{Zr}_2\text{O}_7$. $\text{Nd}_2\text{Zr}_2\text{O}_7$ is a Pyrochlore material which exhibits “momentum fragmentation”, realising a ground state with “all-in all-out” (AIAO) magnetic order, with a dynamical spin liquid encoded in its excitations [2, 3]. Following [3], its effective Hamiltonian can be written as

$$\mathcal{H}_{\text{NZO}} = \sum_{\langle ij \rangle} [\tilde{J}_x \tilde{\tau}_i^{\tilde{x}} \tilde{\tau}_j^{\tilde{x}} + \tilde{J}_y \tilde{\tau}_i^{\tilde{y}} \tilde{\tau}_j^{\tilde{y}} + \tilde{J}_z \tilde{\tau}_i^{\tilde{z}} \tilde{\tau}_j^{\tilde{z}}], \quad (37)$$

where $\tilde{\tau}_i^{\tilde{\alpha}}$ are the spin-half operators with a global rotation. Up to a constant coefficient, the magnetic moment on lattice site i is given by

$$\mathbf{m}_i = \cos \theta \mathbf{m}_i^{\tilde{z}} + \sin \theta \mathbf{m}_i^{\tilde{x}}, \quad (38)$$

where $\mathbf{m}_i^{\tilde{\alpha}}$ is defined as

$$\mathbf{m}_i^{\tilde{\alpha}} = \tilde{\tau}_i^{\tilde{\alpha}} \hat{\mathbf{z}}_i. \quad (39)$$

The values of the parameters

$$\tilde{J}_x = 0.103 \text{ meV}, \quad \tilde{J}_y = 0.0 \text{ meV}, \quad \tilde{J}_z = -0.047 \text{ meV}, \quad \theta = 0.83, \quad (40)$$

are taken from [3].

Our aim is to reproduce the spin-spin correlation measured by neutron scattering

$$S^{\text{theory}}(\mathbf{q}, \omega) = \cos^2 \theta S^{\tilde{z}}(\mathbf{q}, \omega) + \sin^2 \theta S^{\tilde{x}}(\mathbf{q}, \omega), \quad (41)$$

where

$$S^{\tilde{\alpha}}(\mathbf{q}, \omega) = \int dt e^{-i\omega t} (\delta_{\beta\gamma} - \frac{q_\beta q_\gamma}{q^2}) \langle m_\beta^{\tilde{\alpha}}(\mathbf{q}) m_\gamma^{\tilde{\alpha}}(-\mathbf{q}) \rangle. \quad (42)$$

Here $\tilde{\alpha} = \tilde{z}, \tilde{x}$ denote different vector fields, and $\beta, \gamma = x, y, z$ denote the spatial components.

The essential physics of fragmentation is that $\mathbf{m}_i^{\tilde{z}}$ forms the AIAO order, and it pushes the $\mathbf{m}_i^{\tilde{x}}$ fluctuation to finite energy. Furthermore, the fluctuation of $\mathbf{m}_i^{\tilde{x}}$ obeying $\nabla \cdot \mathbf{m}_i^{\tilde{x}} = 0$ decouples dynamically, and forms a flat band. The divergence-free condition gives rise to pinch points on the band. This is exactly the physics of $\mathbf{m}_\nu^{\text{curl}}$ in the Main Text.

From the Main Text we also know that the divergence-full part $\nabla \times \mathbf{m}_i^{\tilde{x}} = 0$ of its fluctuation will form another band that is curved, and encodes the perpendicular pinch points as half moons. In this case the system is in three-dimensional, but that does not make any qualitative difference.

Therefore, we can conclude that $S^{\tilde{z}}(\mathbf{q}, \omega)$ contains the Bragg peaks of the ordered $\mathbf{m}_i^{\tilde{z}}$. We can ignore them. $S^{\tilde{x}}(\mathbf{q}, \omega)$ has the structure of the spin-spin correlation we discussed in the Main Text. It contains a flat band with pinch points, and a curved band with half moons.

Let us now compute $S^{\tilde{x}}(\mathbf{q}, \omega)$ quantitatively. Applying the Helmholtz decomposition [cf. Ref.[3]], the vector fields $\mathbf{m}^{\tilde{\alpha}}$, $\alpha = x, y$, can be written as

$$\mathbf{m}^{\tilde{\alpha}} = \mathbf{m}^{\tilde{\alpha}, \text{div}} + \mathbf{m}^{\tilde{\alpha}, \text{curl}} = \nabla a^{\tilde{\alpha}} + \nabla \times \mathbf{A}^{\tilde{\alpha}}. \quad (43)$$

Their equations of motion are [3]:

$$\partial_t \mathbf{A}^{\tilde{x}} = -(3|\tilde{J}_z| - 1\tilde{J}_y)\mathbf{A}^{\tilde{y}}, \quad (44)$$

$$\partial_t \mathbf{A}^{\tilde{y}} = (3|\tilde{J}_z| - 1\tilde{J}_x)\mathbf{A}^{\tilde{x}}, \quad (45)$$

$$\partial_t a^{\tilde{x}} = -(\frac{\tilde{J}_y}{2}\nabla^2 + (3|\tilde{J}_z| - 1\tilde{J}_y))a^{\tilde{y}}, \quad (46)$$

$$\partial_t a^{\tilde{y}} = (\frac{\tilde{J}_x}{2}\nabla^2 + (3|\tilde{J}_z| - 1\tilde{J}_x))a^{\tilde{x}}. \quad (47)$$

From Eqs. (44),(45), we know that $\mathbf{m}^{\tilde{\alpha},\text{curl}}$ form a flat band with pinch points at energy

$$\omega_1 = \left[(3|\tilde{J}_z| - \tilde{J}_x)(3|\tilde{J}_z| - \tilde{J}_y) \right]^{1/2}. \quad (48)$$

From Eqs. (46),(47), we know that $\mathbf{m}^{\tilde{\alpha},\text{div}}$ form a curved band with half moons. Its dispersion relation is

$$\begin{aligned} \omega_2(\mathbf{q}) &= \left[(\tilde{J}_x \mathbf{q}^2/2 + 3|\tilde{J}_z| - \tilde{J}_x)(\tilde{J}_y \mathbf{q}^2/2 + 3|\tilde{J}_z| - \tilde{J}_y) \right]^{1/2} \\ &\approx [(3|\tilde{J}_z| - \tilde{J}_x)(3|\tilde{J}_z| - \tilde{J}_y)]^{1/2} \times \\ &\quad \left[1 + \frac{\tilde{J}_x(3|\tilde{J}_z| - \tilde{J}_y) + \tilde{J}_y(3|\tilde{J}_z| - \tilde{J}_x)}{4(3|\tilde{J}_z| - \tilde{J}_x)(3|\tilde{J}_z| - \tilde{J}_y)} \mathbf{q}^2 \right]. \end{aligned} \quad (49)$$

Combining the band dispersion relations Eqs.(48),(49), and the knowledge of the spectral weight distributions on these bands from the Main Text Eq. (8,12), one can write down $S^{\tilde{x}}(\mathbf{q}, \omega)$ entirely. For $\mathbf{q} = (0, 0, 2) + (\delta h, \delta h, \delta l)$, we have

$$S^{\text{theory}}(\mathbf{q}, \omega) = \sin^2 \theta S^{\tilde{x}}(\mathbf{q}, \omega) = \delta(\omega - \omega_1) \times \sin^2 \theta (1 + \frac{(\delta h)^2}{(\delta h)^2 + (\delta l)^2}) + \delta(\omega - \omega_2(\mathbf{q})) \times \sin^2 \theta \frac{(\delta l)^2}{(\delta h)^2 + (\delta l)^2}. \quad (50)$$

Finally let us fit the theoretical results with experiments. The major issues are that in experiment there is a strong incoherent background signal, and the experimental resolution is finite. For the first issue we introduce a Gaussian background

$$I^{\text{bkg}}(\mathbf{q}, \omega) = A \exp(-\frac{\omega^2}{\sigma^2}). \quad (51)$$

For the second issue we introduce a Gaussian convolution of $S^{\text{theory}}(\mathbf{q}, \omega)$ with the same width σ

$$I^{\text{theory}}(\mathbf{q}, \omega) = \int d\omega' B \exp(-\frac{(\omega - \omega')^2}{\sigma^2}) \times S^{\text{theory}}(\mathbf{q}, \omega'), \quad (52)$$

and use the sum of the two

$$I^{\text{exp}}(\mathbf{q}, \omega) = I^{\text{bkg}}(\mathbf{q}, \omega) + I^{\text{theory}}(\mathbf{q}, \omega) \quad (53)$$

to represent the experimental results.

There are three fitting parameters A, B, σ in $I^{\text{exp}}(\mathbf{q}, \omega)$. To determine them, we visually fit it against the red curve in Fig. 4(b) of [4], and obtain

$$A = 1.0 \text{ meV}, B = 0.24, \sigma = 0.027 \text{ meV}. \quad (54)$$

There is no freely adjustable parameters left. $I^{\text{exp}}(\mathbf{q} = (0.9, 0.9, 0.9), \omega)$ as a function of ω is plotted in Fig. 3, to be compared to Fig. 4(b) of [4].

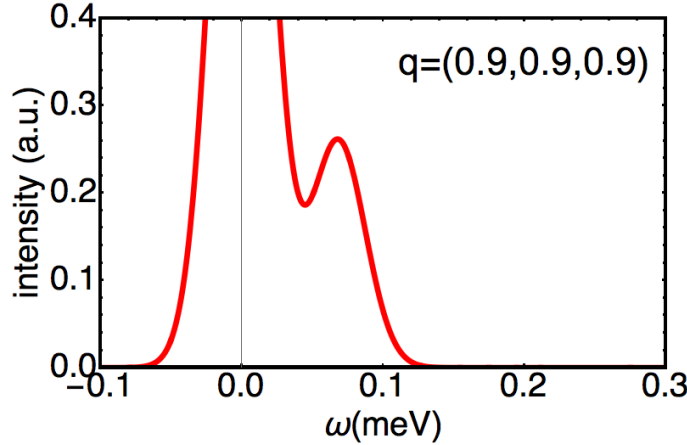


FIG. 3. Signal strength $I^{\text{exp}}(\mathbf{q}, \omega)$ at $\mathbf{q} = (0.9, 0.9, 0.9)$ computed by the field theory with proper Gaussian evolutions and background [cf Eq. (53)], fitted against the red curve of Fig. 4(b) of [4].

With the full expression of $I^{\text{exp}}(\mathbf{q}, \omega)$ given, we proceed to plot the inelastic neutron scattering results, which are shown in Fig. 4 of the Main Text. They are in good agreement of Fig. S3 of the Supplementary Information of [4], for regions close to the Γ -points.

VII. NUMERICAL SIMULATION

A. Classical Monte Carlo Simulations

Numerical simulations have been performed for classical vector spins of length $|\mathbf{S}| = 1$, by evaluating Eq. (1) for $H = 0$. Monte Carlo (MC) simulations were performed by using the local heat-bath algorithm [5, 6], in combination with parallel tempering [7, 8], and over-relaxation [9] on systems with 10800 spins. A single hybrid MC step consists of N local heat-bath updates on randomly chosen sites, followed by two over-relaxation steps for the whole lattice, each comprising a π -rotation of each spin about their local exchange field. Simulations were performed in parallel for replicas at 400 different temperatures, with replica-exchange initiated by the parallel tempering algorithm every 100th MC step. Thermodynamic quantities were averaged over 10^6 statistically independent samples, after simulated annealing (10^6 MC steps) and thermalisation (10^6 MC steps). In addition, all measured quantities have been averaged over 20 independent simulations.

B. Molecular Dynamics

Molecular dynamics (MD) simulations are based on the numerical integration of the Heisenberg equations of motion

$$\frac{d\mathbf{S}_i}{dt} = \frac{i}{\hbar} [\mathcal{H}, \mathbf{S}_i] = J \sum_j \mathbf{S}_j \times \mathbf{S}_i, \quad (55)$$

where j accounts for all nearest-neighbouring sites of i . Spin configurations for MD simulations were taken from a thermal ensemble of spins generated by classical MC simulations of \mathcal{H} [Eq. (1)], for temperatures as indicated in Fig. 3 (Main Text). Numerical integration of Eq. (55) has carried out using a 4th order Runge-Kutta algorithm, as described in [10, 11].

The dynamical structure factor

$$S(\mathbf{q}, \omega) = \frac{1}{\sqrt{N_t N}} \sum_{i,j}^N e^{i\mathbf{q}(\mathbf{r}_i - \mathbf{r}_j)} \sum_n^{N_t} e^{i\omega n\delta t} \langle \mathbf{S}_i(0) \cdot \mathbf{S}_j(t) \rangle, \quad (56)$$

was calculated by using a Fast Fourier Transform (FFT) [12], and has been averaged over spin dynamics obtained from 1000 independent initial spin configurations. MD simulations shown in Fig. 3 (Main Text) were performed for

$N_t = 600$ time steps and maximally resolvable frequency limit of $\omega_{\max} = 6$ meV. Each resolving time-increment δt can be obtained by

$$\delta t = \frac{t_{\max}}{N_t} = \frac{2\pi}{\omega_{\max}} . \quad (57)$$

Additionally, the time sequence of spin configurations has been multiplied by a Gaussian envelop, in order to avoid numerical artefacts, like the Gibbs phenomenon [1] coming from discontinuities of the finite time-window at $t = 0$ and $t = t_{\max}$. This imposes a Gaussian energy convolution on the numerically-obtained $S(\mathbf{q}, \omega)$ in Fig. 3 (Main Text) of FWHM ≈ 0.03 meV.

[1] George B. Arfken and Hans J. Weber, *Mathematical Methods for Physicists – International Edition*, 4th ed. (Academic Press, INC, 1995).

[2] S. Petit, E. Lhotel, B. Canals, M. Ciomaga Hatnean, J. Ollivier, H. Mutka, E. Ressouche, A. R. Wildes, M. R. Lees, and G. Balakrishnan, “Observation of magnetic fragmentation in spin ice,” *Nat Phys* **12**, 746–750 (2016).

[3] Owen Benton, “Quantum origins of moment fragmentation in $\text{Nd}_2\text{Zr}_2\text{O}_7$,” *Phys. Rev. B* **94**, 104430 (2016).

[4] S. Petit, E. Lhotel, B. Canals, M. Ciomaga Hatnean, J. Ollivier, H. Mutka, E. Ressouche, A. R. Wildes, M. R. Lees, and G. Balakrishnan, “Observation of magnetic fragmentation in spin ice,” *Nature Physics* **12**, 746–750 (2016), [arXiv:1603.05008](https://arxiv.org/abs/1603.05008).

[5] J. A. Olive, A. P. Young, and D. Sherrington, “Computer simulation of the three-dimensional short-range heisenberg spin glass,” *Phys. Rev. B* **34**, 6341–6346 (1986).

[6] Y Miyatake, M Yamamoto, J J Kim, M Toyonaga, and O Nagai, “On the implementation of the ‘heat bath’ algorithms for monte carlo simulations of classical heisenberg spin systems,” *Journal of Physics C: Solid State Physics* **19**, 2539 (1986).

[7] Robert H. Swendsen and Jian-Sheng Wang, “Replica monte carlo simulation of spin-glasses,” *Phys. Rev. Lett.* **57**, 2607–2609 (1986).

[8] David J. Earl and Michael W. Deem, “Parallel tempering: Theory, applications, and new perspectives,” *Phys. Chem. Chem. Phys.* **7**, 3910–3916 (2005).

[9] Michael Creutz, “Overrelaxation and monte carlo simulation,” *Phys. Rev. D* **36**, 515–519 (1987).

[10] William H. Press, Saul A. Teukolsky, William T. Vetterling, and Brian P. Flannery, *Numerical Recipes 3rd Edition: The Art of Scientific Computing*, 3rd ed. (Cambridge University Press, New York, NY, USA, 2007).

[11] Ernst Hairer, Gerhard Wanner, and Syvert P. Nørsett, *Solving Ordinary Differential Equations I – Nonstiff Problems* (Springer Berlin Heidelberg, 1993).

[12] Matteo Frigo and Steven G. Johnson, “The design and implementation of FFTW3,” *Proceedings of the IEEE* **93**, 216–231 (2005), special issue on “Program Generation, Optimization, and Platform Adaptation”.